Volume 1 | Number 1 | Jan 2013 | Pages 1–100

Journal of
Materials Chemistry A

Materials for energy and sustainability
www.rsc.org/materialsA

ROYAL SOCIETY
OF CHEMISTRY

ROYAL SOCIETY
OF **CHEMISTRY**

www.rsc.org/materialsA

Journal of Materials Chemistry A

ARTICLE

Reduced Graphene Oxide Decorated with CuO-ZnO Hetero-Junctions: towards High Selective Gas-Sensing Property to Acetone

Chao Wang, Junwu Zhu*, Shiming Liang, Huiping Bi, Qiaofeng Han, Xiaoheng Liu, Xin Wang*

The development of efficient gas sensor device with high sensitivity, well selectivity and excellent stability is necessary to satisfy future societal and environmental needs. Herein, a one-step hydrothermal strategy is developed for the synthesis of CuO-ZnO/reduced graphene oxide (rGO) ternary composite. Compositional, morphological and structural analyses demonstrate the successfully anchoring of nano-scale p-n junctions between CuO and ZnO nanoparticles on rGO sheets. The obtained CuO-ZnO/rGO ternary composite exhibits outstanding sensing properties to acetone (the gas response value reaches 9.4 towards 10 ppm of acetone), almost 1.5 times and 2.0 times higher than CuO-ZnO and ZnO/rGO, respectively. More significantly, the ternary composite presents weaker sensing performance to ethanol, showing superior performance for effectively distinguishing acetone and ethanol. Moreover, the ternary composite exhibits well selectivity towards acetone vapor (about 6-41 times greater than that of other tested vapors). These findings highlight beneficial synergistic effects originated from large numbers of valid p-n junctions of CuO-ZnO and superior substrate characteristics of rGO sheets.

Introduction

Gas sensors based on semiconducting metal oxides (MOX) are the most emerged sensor systems, and have drawn considerable attention due to the increasing concerns for pollution and effects on health. So far, several types of gas sensing technologies, including optical detection,[1] electrochemical detection and resistive devices,[2,3] are being developed. However, in consideration of practical application, developing an efficient gas sensor device with high sensitivity, selectivity and stability (the well known "3S" of a gas sensor) is highly desirable.[4]

Acetone is a volatilize-easily and potentially hazardous chemical solvent in industry or laboratory,[5] thus detecting acetone in workplace makes much sense to human safety and health. Apart from that, being a significant index for the diagnosis of human diseases,[6,7] as well as a referential data for food quality,[8] the detection of acetone concentration is also of great necessity. At present, various acetone sensors based on semiconductor oxides have been fabricated.[9-11] Nevertheless, due to analogous chemical character, the sensing behaviors of ethanol and acetone are similar in most investigations.[11,12] So it still remains a great challenge to develop a highly selective gas sensor to effectively distinguish acetone and ethanol.

Actually, the concept of using p and n-type semiconductor as well as their mixtures to improve sensor performance has been reported.[13-15] In General, for p and n-type mixtures, there are primarily two strategies, mixing p- and n-type powders or creating a p-n diode-type junction.[13] Thereinto, CuO-ZnO hetero-contact based gas sensor has been studied to detect several reducing gases and vapors. For instance, Yu et al. found that the response towards CO (1000 ppm) at room temperature can be enhanced by loading CuO-ZnO with 0.4 % Pt.[16] Kim et al. developed a glucose-mediated hydrothermal method to prepare nano-scale p(CuO)-n(ZnO) junctions, which presented high responses to H2S gas.[17] Moreover, Huang et al. prepared porous flower-like CuO/ZnO nanostructures by using a facile chemical solution method combined with subsequent calcination, exhibiting a higher response and lower working temperature towards several organic vapors.[18] However, due to weak mechanical contact, general hetero-contact type sensors have poor reliability, which may affect the stability of sensors. Besides, the p-type or n-type nanoparticles are easy to aggregate and form p-p junctions or n-n junctions ultimately.[19] Therefore, a substrate with sufficient conductivity and chemical stability is in demand to ensure the formation of valid p-n junctions.

Recently, several graphene and reduced graphene oxide (rGO) based composites have been synthesized for improving gas sensing properties owing to the high specific surface area, excellent thermal stability and high intrinsic electron mobility of graphene sheets.[20-24] Especially, rGO sheet has been accepted to be an outstanding substrate to immobilize nanoparticles. Unfortunately, up to now, the

simultaneous deposition of p- and n-type metal oxides on rGO sheets for acetone gas sensor has been rarely reported.

Herein, we reported a one-step hydrothermal method to deposit p-type CuO and n-type ZnO on surfaces of rGO sheets for the synthesis of CuO-ZnO/rGO ternary composite. The incorporation of CuO-ZnO with rGO distinctly improved the gas sensing response to acetone. More significantly, this CuO-ZnO/rGO composite exhibited weak gas sensing signal towards ethanol, which makes the ternary composite more suitable for effectively distinguishing between acetone and ethanol. This work would provide a wider space for gas sensing application of graphene-based composites.

Results and discussion

The typical XRD patterns of as-synthesized products are shown in Fig. 1a. As displayed in the patterns of GO, the most intensive peak at around $2\theta=10.48°$ corresponds to the (001) reflection of GO, and the interlayer spacing (0.84 nm) is much larger than that of pristine graphite (0.34 nm), because of the introduction of oxygen-containing functional groups.[25] As to the obtained composites, all peaks can be assigned to CuO (JCPDS no. 89-5898) or ZnO (JCPDS no. 79-0206), indicating that there is no chemical reaction between the two oxides during the whole process. The absence of any peak shift for characteristic peaks of ZnO or CuO in CuO-ZnO/rGO further excludes the possibility that CuO and ZnO nanocrystals incorporate into each other's lattices, which is not conducive to form p-n

Fig. 1. (a) XRD patterns of CuO-ZnO/rGO, CuO-ZnO, ZnO/rGO and GO; (b) Raman spectra of GO, CuO-ZnO/rGO and CuO-ZnO.

junctions. Notably, it is hard to find the reflection peaks of layered GO (001) as well as bulk graphite (002, around $2\theta=26°$) in all rGO-based composites, which can be explained by two reasons. On the one hand, due to the small quantity of rGO in CuO-ZnO/rGO composite (approximately 5 wt%), the most of rGO sheets are covered by CuO-ZnO nanoparticles. Consequently, the relatively strong characteristic peak intensities of ZnO as well as CuO nanoparticles, and the small amount of GO in composite contribute to the hard observation of rGO peak in XRD patterns; On the other hand, the *in-situ* formed CuO-ZnO nanoparticles might attach onto surfaces of rGO sheets and prevent their aggregation and restacking, which could also weaken the diffraction peak of rGO.[25,26]
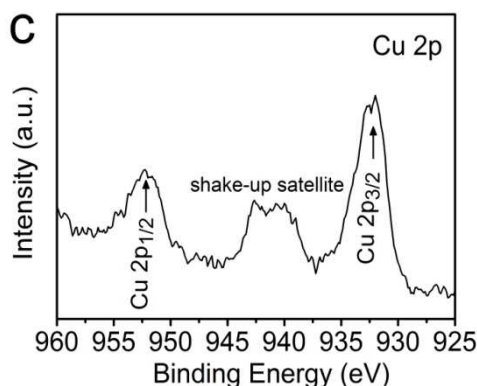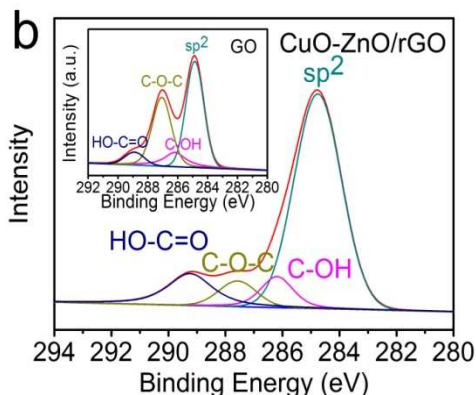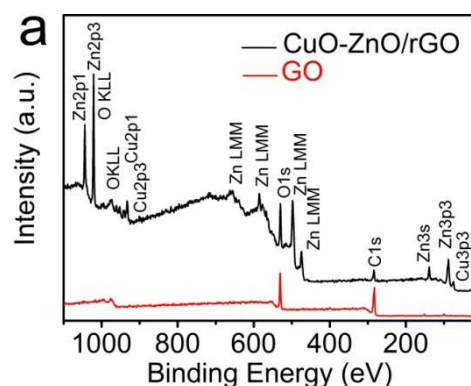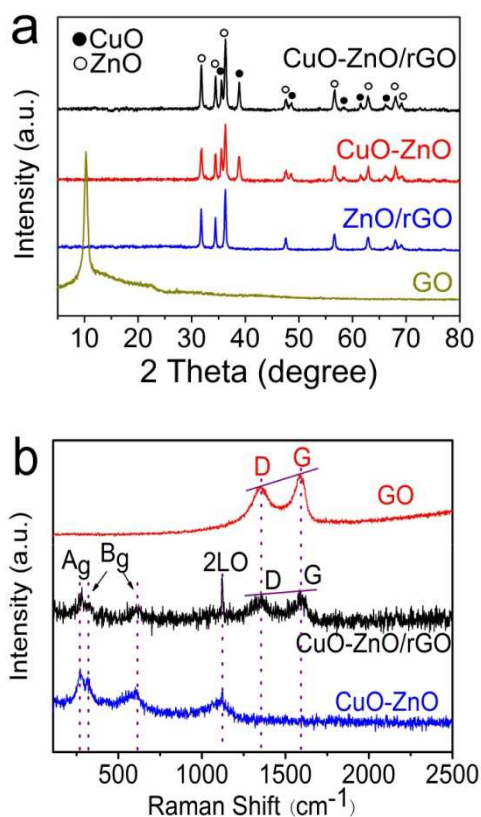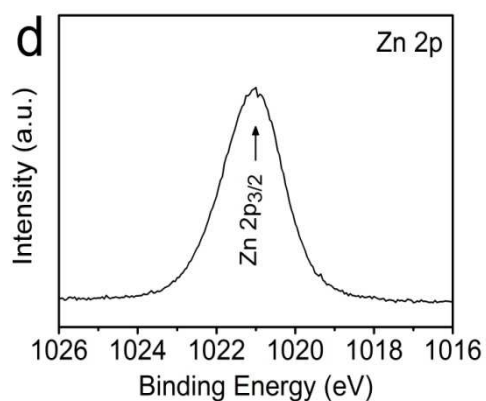
Fig. 2 XPS survey of (a) whole scan spectrum; (b) deconvoluted C 1s of CuO-ZnO/rGO, the insert of (b) is deconvoluted C 1s of GO; (c) Cu 2p of CuO-ZnO/rGO; (d) Zn 2p of CuO-ZnO/rGO.

Raman spectroscopy is one of the most sensitive and informative techniques used for the characterization of carbon-based materials. As showed in Fig. 1b, it is clear that GO exhibits two main intrinsic peaks: the D band (at 1358 cm^{-1}) arising from a breathing mode of κ-point photons of A_{1g} symmetry; the G band (at 1584 cm^{-1}) originating from the first-order scattering of E_{2g} phonon of sp^2 carbon atoms.[27] As to CuO-ZnO/rGO, two prominent peaks of rGO still exist and appear at around 1360 and 1583 cm^{-1}. Notably, there is an increase in I_D/I_G (intensity ratio of D and G line) of CuO-ZnO/rGO (0.97) compared with that of GO (0.83), suggesting the decrease of average size of sp^2 domains upon the hydrothermal reduction and the occurrence of GO reduction.[28] The Raman spectra of CuO-ZnO/rGO and CuO-ZnO show similar features in the range of 100–1200 cm^{-1}, which can be assigned to one A_g (at 272 cm^{-1}), two B_g (at 324 and 594 cm^{-1}) of CuO and 2LO region (at 1124 cm^{-1}) of ZnO, respectively.[29,30] The XRD and Raman results indicate that exfoliated rGO sheets and CuO-ZnO nanocrystals coexist in the prepared composites.

The surface composition and element analysis of the CuO-ZnO/rGO and GO were further investigated by XPS technique. As showed in Fig. 2a, all peaks can be ascribed to Zn, Cu, O and C elements, confirming the formation of CuO-ZnO/rGO without any impurities. In Fig. 2b, the C 1s spectra of CuO-ZnO/rGO could be deconvoluted into four peaks at 284.8 (C–C), 286.2 (C-OH), 287.6 (C-O-C) and 289.2 eV (HO-C=O). Compared with C 1s spectrum of GO (the insert in Fig. 2b), the intensity of some oxygen-containing (especially epoxy groups) in the CuO-ZnO/rGO composite experienced a considerable reduction. This result shows that, *via* 24 h hydrothermal process at 180 °C, GO has been reduced to rGO with little amount of residual oxygenic groups,[31] which is consistent with the Raman results. The Cu 2p spectrum (Fig. 2c) exhibits a 2p$_{3/2}$ peak at 932.5 eV, 2p$_{1/2}$ peak at 932.5 eV and strong shake-up satellite peaks at about 941.0 eV, which further confirms the presence of CuO and rules out the possible existence of Cu$_2$O phase.[32,33] Similarly, the peak at 1021.0 eV can be assigned to Zn

2p$_{3/2}$ (Fig. 2d), and it is in agreement with the standard spectrum of ZnO.[15] All the XPS spectra in Fig. 2 evidence that this one-step hydrothermal method is a feasible way for reducing GO and incorporating nanoparticles on rGO sheets, simultaneously.
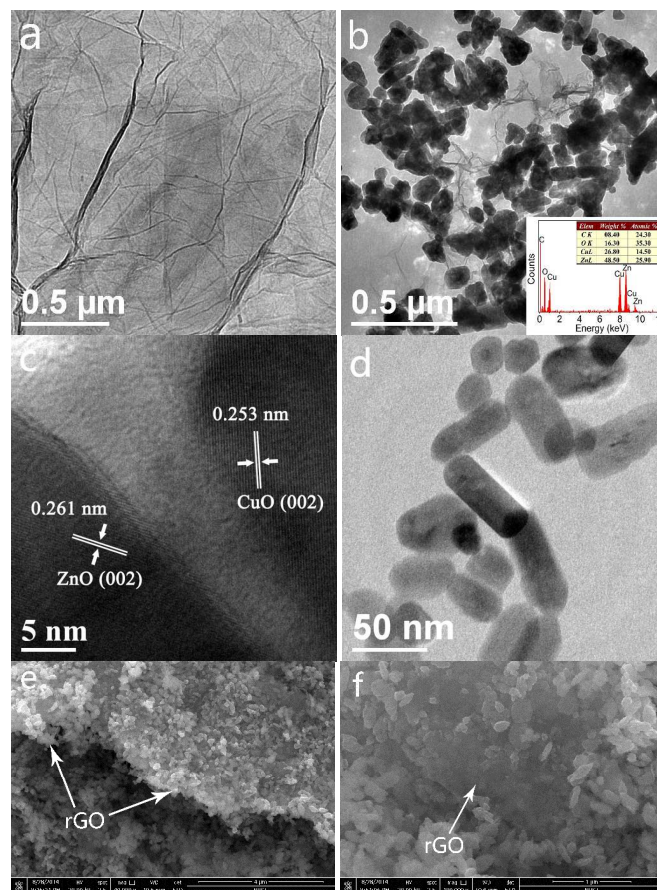

Fig. 3 TEM or HRTEM images of (a) GO, (b, c) CuO-ZnO/rGO and (d) CuO-ZnO, the insert of (b) is EDS spectrum of CuO-ZnO/rGO; (e, f) FESEM of CuO-ZnO/rGO.

The morphologies of obtained samples were investigated by TEM and FESEM. As showed in Fig. 3a, pristine GO sheets possess many wrinkles on their surfaces and edges, which endow them with a large specific surface area. The dramatic differences in microstructure between GO (Fig. 3a) and CuO-ZnO/rGO (Fig. 3b) suggest that rGO sheets have been successfully decorated with CuO and ZnO nanoparticles, and this consequence can be further supported by energy dispersive X-ray analysis (the insert in Fig. 3b). More TEM images of CuO-ZnO/rGO can be seen in Supporting Information of Fig. S1a and 1b. For the sake of differentiating the CuO and ZnO nanoparticles from the TEM images, the TEM of CuO/rGO (Fig. S1c) and ZnO/rGO (Fig. S1d) binary composites were investigated. As can be seen from Fig. S1c, the CuO nanoparticles show a granule shape with average sizes of 80 nm. Similarly, the typical image of ZnO/rGO nanocomposite is presented in Fig. S1d. The ZnO consists of the distinctive rod-liked nanoparticle with approximately 100 nm in length and 40 nm in width. Consequently, as to CuO-ZnO/rGO (Fig. 3b; Supporting Information, Fig. S1a and 1b), the granular-

shaped CuO and rod-liked ZnO nanoparticles could be distinguished on rGO sheets (the ZnO marked by the white arrows, and the CuO labeled by the white circles in Fig. S1a, Supporting Information). However, it is not as easy to distinguish the boundary between CuO and ZnO particles. This can be explained by that the rGO sheets can act as nucleation centers to promote the close contact between CuO and ZnO nanoparticles, and sequentially bring about a mild agglomeration of ZnO-CuO nanoparticles, which might facilitate the formation of more valid p-n junctions of CuO-ZnO/rGO. Moreover, from the HRTEM image of CuO-ZnO/rGO (Fig. 3c), two kinds of lattice spacing can be seen clearly. The spacing of 0.253 nm corresponds to the (002) planes of p-typed CuO, while the lattice spacing of 0.261 nm can perfectly match with the (002) plane of n-type ZnO. The HRTEM image, combined with the previous results, indicates the formation of p-n junctions on rGO sheets. Moreover, for comparison, the CuO-ZnO nanoparticles were also prepared using a similar process in the absence of rGO. Interestingly, in contrast to CuO-ZnO/rGO, the CuO-ZnO nanoparticles (Fig. 3d) contact with each other more loosely. We could speculate that the loose contacts between CuO and ZnO may reduce the amount as well as the stability of valid p-n junctions. It is worth mentioning that, in the presence of rGO, the average size of CuO and ZnO nanocrystals increases, accompanying by the change of morphology, which is consistent with previous reports.[34-36] It is reasonable to propose that the rGO sheets play a role in growth of nanocrystals and act as nucleation centers and templates, which can make the nanocrystals grow on the specific sites and directions, leading to the change of morphology and close contact between CuO and ZnO nanoparticles. The morphology of CuO-ZnO/rGO composite was further studied by FESEM. Taking into account the small quantity of rGO in CuO-ZnO/rGO, the most surfaces of rGO sheets have been covered by CuO-ZnO nanoparticles. Even so, the exposed rGO sheets can still be observed in the FESEM images (marked by the white arrows in Fig. 3e, 3f and Fig. S2, Supporting Information).

Generally, the gas response is strongly influenced by temperatures. The function of operating temperatures on sensor response of CuO-ZnO/rGO was investigated (Fig. 4a). It is found that the response to 10 ppm of acetone firstly improved with increasing operating temperatures and reached its maximum at 340 °C, then decreased with further elevating temperatures. This phenomenon can be attributable to kinetics and thermodynamics of gas adsorption and desorption on the surfaces of CuO-ZnO/rGO or other similar semiconducting metal oxides.[4, 18, 37] Obviously, Fig. 4a reveals that 340 °C is the optimum operating temperature for selective detection and rapid sensing behavior of acetone, which is applied in all investigations hereinafter.

Accordingly, the sensing transients to acetone were measured at optimum operating temperature of 340 °C (Fig. 4b). The response value to 10 ppm of acetone was 9.4, indicating that it could be detected at sub-ppm-levels using the CuO-ZnO/rGO based sensor. The process of sensing transients may probably describe as follows: the initial volume of acetone vapor is consumed in establishing the percolation network (as the light magenta region showed in Fig. 4b).[38] It takes 10 to 15 s for complete percolation during the

response value increases from 1 to about 9. After percolation is finished, the gas molecules start adsorbing on surfaces of CuO-ZnO/rGO nanoparticles, leading to a slow increase in response. Subsequently, rapid recovery (as the dark grey region showed in Fig. 4b) happened, which is likely because the breaking of percolation network as gas molecules are swept by purging air.[38] During this desorption process, the sensor rapidly recovers 90 % of its initial response value within approximately 15 s. As showed in insert of Fig. 4b, the sample presents a fast response (10 s) and recovery (14 s) time to acetone. Furthermore, the almost complete recovery of baseline response values at the end of each pulse shows an excellent reversible and repeatable performance, which is a key element for ultimate technological applications.
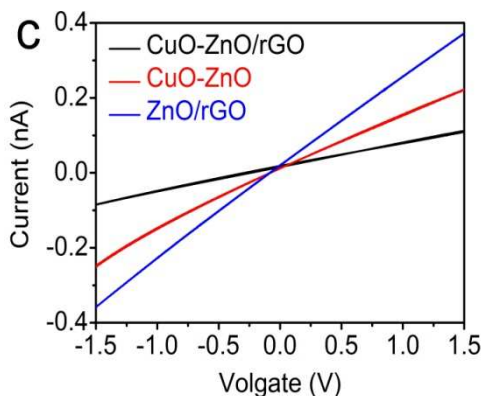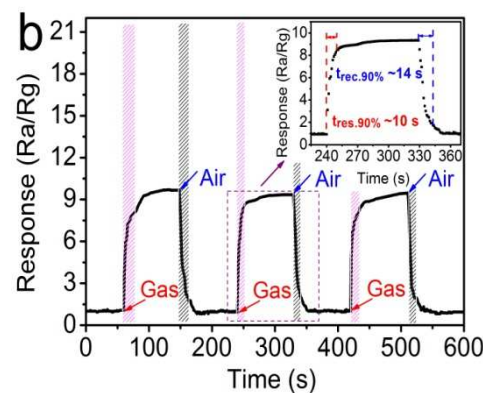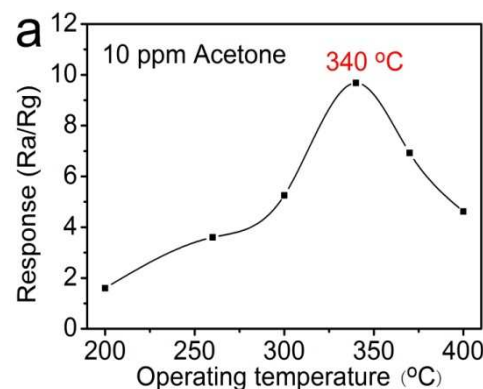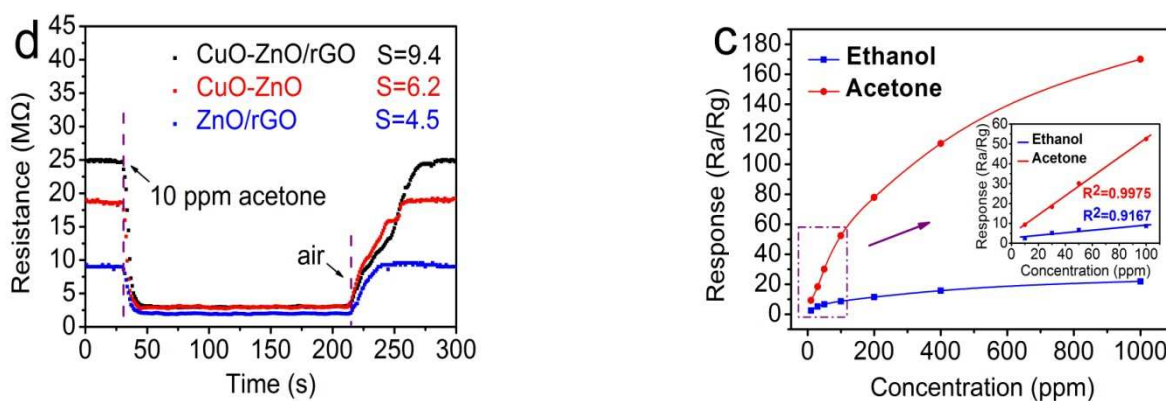
Fig. 4 (a) The response of CuO-ZnO/rGO sensor to 10 ppm of acetone vs. operating temperatures; (b) The response transients of CuO-ZnO/rGO sensor to 10 ppm of acetone, the inset of (b) depicts the details of once adsorption and desorption; (c) Current–voltage (I–V) characteristics of CuO-ZnO/rGO, CuO-ZnO and ZnO/rGO sensors at room temperature; (d) The resistance curves of CuO-ZnO/rGO, ZnO–CuO and ZnO/rGO sensors to 10 ppm of acetone.
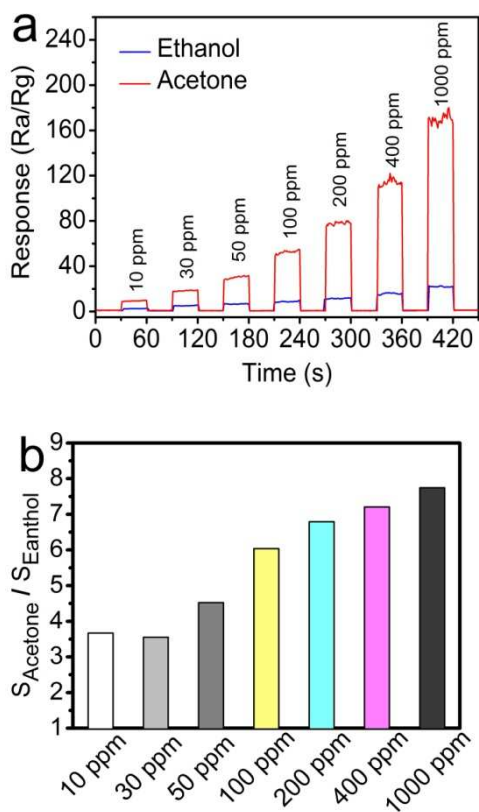

Fig. 5 (a) Sensor responses of CuO-ZnO/rGO towards acetone and ethanol; (b) The $S_{acetone}/S_{ethanol}$ of CuO-ZnO/rGO vs. gas concentrations; (c) The sensitivity tendency of CuO-ZnO/rGO vs. different gas concentrations, the inset shows corresponding calibration curves (10 to 100 ppm); (d) The response of CuO-ZnO/rGO sensor to 100 ppm of various VOCs gases.

Prior to comparing the gas properties of different systems, the current-voltage (I-V) characteristics of different sensors covered with the same weight of samples on ceramic tubes were investigated (Fig. 4c). The linearity and symmetry of I-V curves suggest an ohmic contact between samples and test electrodes. Obviously, compared to CuO-ZnO and ZnO/rGO, the CuO-ZnO/rGO presents the smallest current (the highest resistance). As is well known, CuO as p-type and ZnO as n-type semiconductors might form p-n junctions with electron depletion zones, which will greatly improve the resistance of the whole system. That is, the higher resistance presented by CuO-ZnO/rGO than that of CuO-ZnO precisely illustrates the formation of more hetero-junctions at interface between the two metallic oxides in the presence of rGO. As mentioned in the introduction, general hetero-contact type materials have poor reliability due to weak mechanical contact. Combined with TEM results (Fig. 3), we can draw a conclusion that the CuO and ZnO nanoparticles tend to form enough valid p-n junctions with close contact by using rGO sheets as a stable substrate. All information shows that rGO sheets not only act as a chemical stability substrate but also promote the formation of p-n junctions in CuO-ZnO/rGO ternary composite.

In order to explore the influence of different chemical composition on gas sensitive properties, the resistance transients of CuO-ZnO/rGO, CuO-ZnO and ZnO/rGO towards 10 ppm of acetone at 340 $^{\circ}$C were also investigated (Fig. 4d). Apparently, the resistances of all sensors show a decreased trend when adsorbing acetone vapor (reducing gas), indicating the characteristic of n-typed semiconductors, and these results are in accordance with previous literatures.[18,38] Moreover, the CuO-ZnO/rGO composite shows the highest sensitivity (S=9.4) to 10 ppm of acetone, almost 1.5 times and 2.0 times higher than CuO-ZnO and ZnO/rGO, respectively. Furthermore, the resistance transients of CuO/rGO and rGO were also studied and showed in Supporting Information of Fig. S3. Clearly, both CuO/rGO and rGO present lower response towards acetone compared with the CuO-ZnO/rGO composite, and exhibit the p-type characteristic, which is coincided with published reports.[23,24] Considering distinctive structure of this ternary system, it is speculated that the superior property can be attributed to the introduction of nano-scale p-n junctions and the synergistic effect caused by rGO.

For the sake of comparing the cross-sensitivity of ethanol and acetone, the sensing properties towards two vapors were investigated. As showed in transverse direction of Fig. 5a, the response to acetone rapidly increases with increasing concentration, while the response to ethanol experiences a relatively slow rise. To quantify the selectivity of ternary composite, the ratios of gas response values to acetone and ethanol (labeled as $S_{acetone}/S_{ethanol}$) were calculated (the bar chart in Fig. 5b). As expected, the CuO-ZnO/rGO shows approximately 3.7 times at 10 ppm and 7.7 times at 1000 ppm higher in selectivity towards acetone than that of ethanol, suggesting that the excellent selective detection of acetone can be attained. Table 1 presents comparative analysis of gas selectivity of different materials (all references listed in the table are committed to distinguish between ethanol and acetone). It is evident that the CuO-ZnO/rGO composite can better recognize as well as distinguish these two volatile organic chemicals (VOCs) at sub-ppm-level, and achieve higher selectivity at a relatively lower concentration compared with other materials reported.

Table 1. The comparative analysis of gas selectivity of different materials

Materials	Operating temperature (°C)	$S_{acetone}$: $S_{ethanol}$ at low concentration	$S_{acetone}$:$S_{ethanol}$ at high concentration	Reference
Co-ZnO	360	2.0 at 100 ppm	7 at 35000 ppm	[39]
SnO$_2$-ZnO	300	0.5 at 200 ppm	not reported	[40]
ZnO	300	4.0 at 50 ppm	5.4 at 1500 ppm	[41]
CuO-ZnO/rGO	340	3.7 at 10 ppm	7.7 at 1000 ppm	Current work

The linear fitting method is also useful in helping to understand the selectivity of gas-sensing materials. Fig. 5c shows the gas responses tendency of CuO-ZnO/rGO versus different concentrations of acetone and ethanol. It is seen that the responses rapidly increase with increasing gas concentrations from 10 to 100 ppm. Above 100 ppm, a moderate increase in the response can be observed, which indicates that the gas adsorption gradually reaches its saturation. Moreover, the insert in Fig. 5c exhibits a linear calibration curve in the range of 10-100 ppm. The degree of linear correlation was evaluated by R^2 ($R^2_{acetone}$=0.9975, $R^2_{ethanol}$=0.9167, respectively). Clearly, the response of acetone versus concentration variation (especially at low concentration) is close to linear, which further confirms that the CuO-ZnO/rGO ternary composite is suitable for detecting acetone with high selectivity.

Fig. 5d shows the responses of CuO-ZnO/rGO sensor to several kinds of VOCs: ethanol, ethylene glycol, formic acid, chloroform, acetic acid, propionic acid, methanol, toluene and acetone at 340 ^{o}C. Apparently, the response to acetone vapor is significantly higher than that to the other gases. The response value towards 100 ppm of acetone vapor presents about 6-41 times greater than that of other tested vapors. Consequently, the sensor exhibits superior selective ability to acetone, and can be expected to put into various practical applications.

Actually, high gas sensing performances showed by CuO-ZnO/rGO can be attributed to the introduction of nano-scale p-n junctions onto rGO matrix. First of all, as is can be seen in TEM and SEM images, the most surfaces of rGO sheets are covered by CuO-ZnO nanoparticles because of the small quantity of rGO in CuO-ZnO/rGO composite. Therefore, it is believed that the majority of acetone molecules would contact directly with the CuO-ZnO surface instead of rGO. As reported, metal oxide is considered to be involved in the receptor function while rGO support mainly provides the electronic conduction path.[42] As for ZnO/rGO binary composite, the most widely accepted sensing mechanism could be boiled down to the change on the hole-electron depletion layer.[43,44] However, the sensing mechanism on CuO-ZnO/rGO ternary composite is not identical with ZnO/rGO because of the formation of p-n junctions. In open air, the first depletion layer is due to the adsorption of ionized oxygen (O^{2-}) at surfaces of ZnO nanoparticles (the Step 1. in Fig. 6), while the second depletion layer is caused by the CuO-ZnO hetero-junctions. Both the two electron depletion layers contribute to the improvement of resistivity. At response stage, in addition to the reaction on ZnO surfaces (the Step 2. in Fig. 6), acetone molecule could also adsorb on the active sites of CuO nanoparticles. According to the published reports, in CuO-ZnO composite, the p-type CuO tends to transfer charges from the bulk to the chemisorbed reductive gas molecule.[18,46] Based on the reports by Sahay *et al*. and Tsuboi *et al*.,[37,45] the holes combined with CH$_3$COCH$_3$ are inclined to generate CH$_3$CHO and CH$_3^+$, then the extremely unstable CH$_3^+$

and the generated CH_3CHO will further react with the absorbed oxygen ions (O^{2-}) on the surfaces of n-type ZnO (the Step 3. in Fig. 6). Concisely, the CuO-ZnO hetero-junction active sites convert CH_3COCH_3 with O^{2-} to CH_3CHO, CO_2 and H_2O. Thanks to the existence of p-n junctions, these consumed holes in CuO would quickly be supplemented from the electron depletion layers at p-n junctions. During this process, the holes in CuO-ZnO hetero-structure migrate to CuO across the hetero-contact interface, and the electrons release into the conduction band (CB), increasing the charge carrier concentration and resulting in the declining resistivity. The p-n junctions act as a stable channel for mediating both holes and electrons in CuO-ZnO nanoparticles throughout the course. Compared with the traditional binary system, not only the hole-electron depletion layers on ZnO but also the p-n junctions depletion layers are diminished in CuO-ZnO/rGO, which contribute together to increase the change of resistance. The hypothesis of the diminishing of hole-electron depletion layers is based on the n-type character of CuO-ZnO/rGO, which is in accordance with the experimental phenomena (Fig. 4d). Overall, the addition of p-type CuO into ZnO/rGO can enhance the acetone adsorption kinetics.

Thereby the CuO-ZnO/rGO sensor presents more outstanding sensitivity than that of ZnO/rGO.

It's worth emphasizing that the rGO plays a key role in improving gas sensing properties. Firstly, rGO could provide active sites for the growth and deposition of CuO and ZnO nanoparticles owing to large surface areas.[34] Thus, the special structure endows CuO-ZnO/rGO with more active sites for adsorption and desorption of target gas. Meanwhile, rGO sheets are advantageous to form and stabilize sufficient quantity of nano-scale p-n junctions. Furthermore, rGO has good electrical conductivity, which can facilitate electronic rapid transmission between CuO and ZnO, thus making a contribution to quick response-recovery time.[47] Thanks to the small band gap of rGO, even a slight change of carrier concentration on the rGO surface can also lead to an obvious influence on the electrical conductivity.[48] Such excellent properties of rGO make a great contribution to the improvement of gas sensitive. Therefore, in the presence of rGO, the gas sensing properties of CuO-ZnO/rGO have been greatly enhanced compared with the CuO-ZnO sensor.
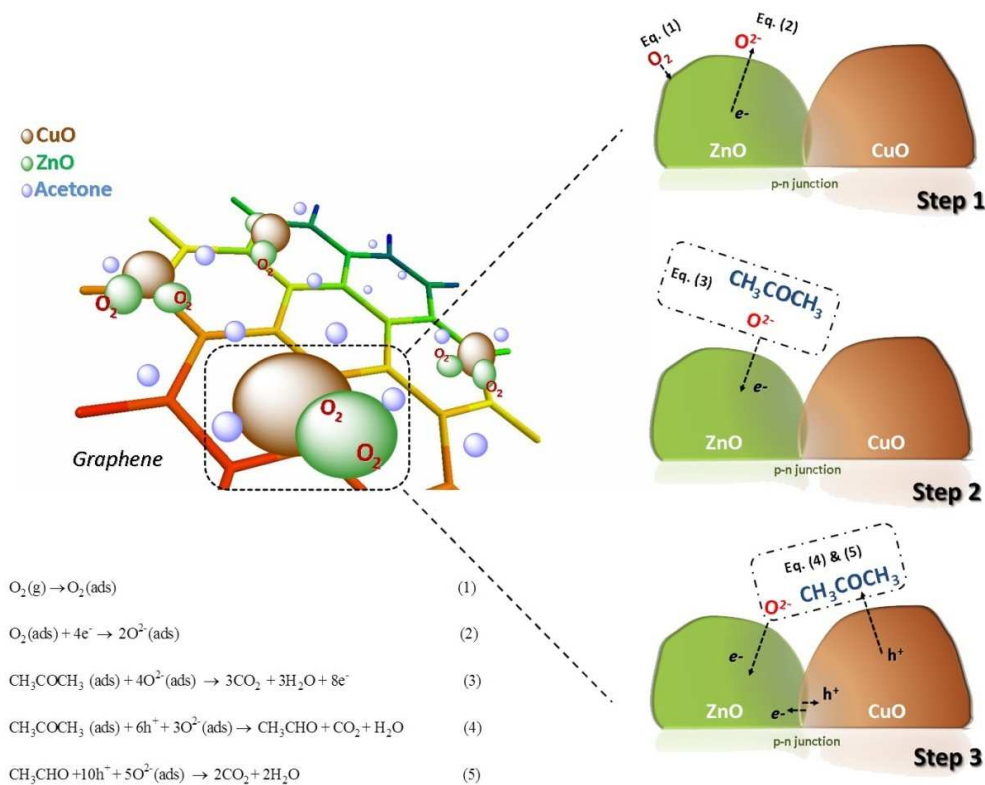

$$O_2(g) \rightarrow O_2(ads) \qquad (1)$$

$$O_2(ads) + 4e^- \rightarrow 2O^{2-}(ads) \qquad (2)$$

$$CH_3COCH_3\,(ads) + 4O^{2-}(ads) \rightarrow 3CO_2 + 3H_2O + 8e^- \qquad (3)$$

$$CH_3COCH_3\,(ads) + 6h^+ + 3O^{2-}(ads) \rightarrow CH_3CHO + CO_2 + H_2O \qquad (4)$$

$$CH_3CHO + 10h^+ + 5O^{2-}(ads) \rightarrow 2CO_2 + 2H_2O \qquad (5)$$

Fig. 6 Schematic diagram of the proposed mechanism of CuO-ZnO/rGO.

Conclusions

In summary, the CuO-ZnO/rGO ternary composite was successfully prepared through a one-step hydrothermal process, forming valid p-n junctions between CuO and ZnO nanoparticles

with the aid of rGO sheets. Anchoring the CuO and ZnO nanoparticles onto rGO sheets not only provides more p-n junctions, but also significantly improves the gas sensing response towards acetone. More significantly, this composite presents superior ability for effectively distinguishing between acetone and ethanol. The large

specific surface area, thermal stability and high intrinsic electron mobility of rGO sheets are able to stabilize the sufficient quantity of effective nano-scale p-n junctions between CuO-ZnO, endowing the CuO-ZnO/rGO composite sensor with excellent sensitivity and selectivity to acetone vapor. This result provides a facile and effective approach to prepare graphene-based composites with enhanced gas sensing properties.

Experimental Section

Synthesis of CuO-ZnO/rGO ternary composite.

Graphene oxide (GO) was prepared from flake graphite (400 mesh) by a modified Hummers method as described previously.[49,50] The CuO-ZnO/rGO ternary composite was synthesized by an *in situ* hydrothermal growth process. In a typical procedure, GO dispersion (50 mL, 0.28 mg·mL^{-1}) was obtained after ultrasonication for 30 min in DI water. Subsequently, Cu(OAc)$_2$·H$_2$O (0.233 g) and Zn(NO$_3$)$_2$·6H$_2$O (0.637 g) were dissolved in DI water (20 mL), and then added to the above GO dispersion. The pH value of the produced mixture was adjusted to 11 using NaOH solution (0.5 M). After that, the mixture was transferred into a 100 mL of Teflon-lined autoclave and heated at 180 °C for 24 h. After being cooled to room temperature, the formed precipitate was centrifuged, washed with deionized water and ethanol, and dried at 60 °C overnight. The forming process of CuO-ZnO/rGO composite can be illustrated in Fig. S4 (Supporting Information). For comparison, CuO-ZnO, ZnO/rGO, CuO/rGO and rGO were prepared using a similar procedure.

Characterization of Materials.

The X-ray diffraction (XRD) analyses were recorded on a Bruker D8 advance X-ray diffractometer using Cu Kα radiation (λ ≈ 1.54 Å) with scanning angle 2θ ranging from 5° to 80°. Raman measurements were tested by a Renishaw inVia Reflex Raman microscope with a 514.5 nm wavelength as incident laser. The surface contents of samples were analyzed by a PHI QUANTERA II X-ray photoelectron spectroscopy (XPS), using Mg Kα (h*ν* = 1253.6 eV) X-ray as the excitation source. The morphology of as-obtained products was characterized by transmission electron microscopy (TEM, JEOL JEM-2100) and field emission scanning electron microscope (Carl Zeiss AURIGA CrossBeam FIB/SEM). The HRTEM image and X-ray energy dispersive spectroscopy (EDS) were also recorded on a JEOL-2100 transmission electron microscope operating at an accelerating voltage of 200 kV. Electrical properties were tested on a CHI 760D electrochemical workstation (Shanghai CH Instrument company).

Fabrication of gas sensor and response test.

The gas sensing tests were carried on a WS-30A measuring system (Winsen Electronics Co. Ltd.). The fabrication of CuO-ZnO/rGO gas sensors was similar to our previously reported process.[51,52] The as-obtained products (0.1 g) were mixed with terpineol (0.4 g) binder to form a uniform slurry through slightly milling. In order to keep the uniformity of the samples coating and the consistency of the samples quality on every ceramic tube, we adopted the method of brushing each ceramic tube with the same 4 times. A small Ni–Cr resistor coil was placed across the tube as a heater to control the working temperature. For the purpose of eliminating terpineol and improving stability, the obtained sensors were aged at working temperature of 340 °C for 3 h before gas response testing. The voltage applied to the whole circuit was 5 V, and the output voltage (V$_{out}$) was equal to the terminal voltage of load resistor element. The modulation of heating voltage can be used to adjust the operating temperature of sensors. The gas response of sensing materials in this paper was defined as S = Ra/Rg, where Ra is the resistance of sensors in air ambience, and Rg is the resistance in test gas.

Acknowledgements

Notes and references

Key Laboratory for Soft Chemistry and Functional Materials, Nanjing University of Science and Technology, Ministry of Education, Nanjing 210094, China.
*To whom correspondence should be addressed. E-mail address: zhujw@njust.edu.cn.

Electronic Supplementary Information (ESI) available: [The forming process of CuO-ZnO/rGO composite.]. See DOI: 10.1039/b000000x/

1. M. Ando, T. Kobayashi, S. Iijima, and M. Haruta, *Sens. Actuat. B*, 2003, **96**, 589-595.
2. W. G. Planje, G. J. M. Janssen and M. P. de Heer, *Sens. Actuat. B*, 2004, **99**, 544-555.
3. E. Comini, C. Baratto, I. Concina, G. Faglia, M. Falasconi, M. Ferroni, V. Galstyan, E. Gobbi, A. Ponzoni, A. Vomiero, D. Zappa, V. Sberveglieri and G. Sberveglieri, *Sens. Actuat. B*, 2013, **179**, 3-20.
4. E. Comini, L. Ottini, G. Faglia and G. Sberveglieri, *IEEE Sens. J.*, 2004, **4**, 17-20.
5. X. Liu, J. Hu, B. Cheng, H. Qin and M. Jiang, *Sens. Actuators, B*, 2008, **134**, 483-487.
6. N. Makisimovich, V. Vorotyntsev, N. Nikitina, O. Kaskevich, P. Karabun and F. Martynenko, *Sens. Actuat. B*, 1996, **35-36**, 419-421.
7. S. S. Likhodii, K. Musa and S. C. Cunnane, *Clin. Chem.*, 2002, **48**, 115-120.
8. A. M. Taurino, C. Distante, P. Siciliano and L. Vasanelli, *Sens. Actuat. B*, 2003, **93**, 117-125.
9. K. W. Kao, M. C. Hsu, Y. H. Chang, S. Gwo and J. A. Yeh, *Sensors*, 2012, **12**, 7157-7168.
10. L. Qin, J. Xu, X. Dong, Q. Pan, Z. Cheng, Q. Xiang and F. Li, *Nanotechnology*, 2008, **19**, 185705.
11. Zhao, J.; Huo, L. H.; Gao, S.; Zhao, H.; Zhao, J. G. *Sens. Actuat. B*, 2006, **115**, 460-464.
12. Z. Jing and S. Wu, *Mater. Lett*, 2006, **60**, 952-956.

13. C. Sun, G. Maduraiveeran and P. Dutta, *Sens. Actuat. B*, 2013, **186**, 117-125.

14. F. Shao, M. W. G. Hoffmann, J. D. Prades, R. Zamani, J. Arbiol, J. R. Morante, E. Varechkina, M. Rumyantseva, A. Gaskov, I. Giebelhaus, T. Fischer, S. Mathur and F. Hernández-Ramírez, *Sens. Actuat. B*, 2013, **181**, 130-135.

15. D. Bekermann, A. Gasparotto, D. Barreca, C. Maccato, E. Comini, C. Sada, G. Sberveglieri, A. Devi and R. A. Fischer, *ACS Appl. Mat. Interf.*, 2012, **4**, 928-934.

16. M. R. Yu, R. J. Wu and M. Chavali, *Sens. Actuat. B*, 2011, **153**, 321-328.

17. S. J. Kim, C. W. Na, I. S. Hwang and J. H. Lee, *Sens. Actuat. B*, 2012, **168**, 83-89.

18. J. Huang, Y. Dai, C. Gu, Y. Sun and J. Liu, *J. Alloys Compd.*, 2013, **575**, 115-122.

19. J. H. Yu and G. M. Choi, *Sens. Actuat. B*, 1999, 61, 59-67.

20. C. N. R. Rao, A. K. Sood, K. S. Subrahmanyam and A. Govindaraj, *Angew. Chem. Int. Ed.*, 2009, **48**, 7752-7777.

21. N. Chen, X. Li, X. Wang, J. Yu, J. Wang, Z. Tang and S. A. Akbar, *Sens. Actuat. B*, 2013, **188**, 902-908.

22. F. Liu, X. Chu, Y. Dong, W. Zhang, W. Sun and L. Shen, *Sens. Actuat. B*, 2013, **188**, 469-474.

23. S. Mao, G. Lu and J. Chen, *J. Mater. Chem. A*, 2014, **2**, 5573-5579.

24. W. Yuan and G. Shi, *J. Mater. Chem. A*, 2013, **1**, 10078-10091.

25. C. Xu, X. Wang, J. Zhu, X. Yang and L. Lu, *J. Mater. Chem.*, 2008, **18**, 5625-5629.

26. S. Chen, J. Zhu, X. Wu, Q, Han and X. Wang, *ACS Nano*, 2010, **4(5)**, 2822-2830.

27. Y. Guo, S. Guo, J. Ren, Y. Zhai, S. Dong and E. Wang, *ACS Nano*, 2010, **4**, 4001-4010.

28. S. Stankovich, D. A. Dikin, R. D. Piner, K. A. Kohlhaas, A. Kleinhammes, Y. Jia, Y. Wu, S. T. Nguyen and R. S. Ruoff, *Carbon*, 2007, **45**, 1558-1565.

29. J. Zhu, G. Zeng, F. Nie, X. Xu, S. Chen, Q. Han and X. Wang, *Nanoscale*, 2010, **2**, 988-994.

30. J. Calleja and M. Cardona, *Phys. Rev. B: Condens. Matter*, 1977, **16**, 3753-3761.

31. Y. Fu, H. Chen, X. Sun and X. Wang, *Appl. Catal. B*, 2012, **111-112**, 280-287.

32. M. Durando, R. Morrish and A. J. Muscat, *J. Am. Chem. Soc.*, 2008, **130**, 16659-16668.

33. J. Zhu, H. Chen, H. Liu, X. Yang, L. Lu and X. Wang, *Mater. Sci. Eng. A*, 2004, **384**, 172-176.

34. C. Xu, X. Wang, L. Yang and Y. Wu, *J. Solid State Chem.*, 2009, **182**, 2486-2490.

35. S. Chen, J. Zhu, H. Zhou and X. Wang, *RSC Adv.*, 2011, **1**, 484-489.

36. J. Zhu, S. Chen, H. Zhou and X. Wang, *Nano Res.*, 2011, **5**, 11-19.

37. P. P. Sahay, *J. Mater. Sci. Lett.*, 2005, **40**, 4383-4385.

38. G. Singh, A. Choudhary, D. Haranath, A. G. Joshi, N. Singh, S. Singh and R. Pasricha, *Carbon*, 2012, **50**, 385-394.

39. L. Liu, S. Li, J. Zhuang, L. Wang, J. Zhang, H. Li, Z. Liu, Y. Han, X. Jiang and P. Zhang, *Sens. Actuat. B*, 2011, **155**, 782-788.

40. K. W. Kim, P. S. Cho, S. J. Kim, J. H. Lee, C. Y. Kang, J. S. Kim and S. J. Yoon, *Sens. Actuat. B*, 2007, **123**, 318-324.

41. Q. Qi, T. Zhang, L. Liu, X. Zheng, Q. Yu, Y.Zeng and H.Yang, *Sens. Actuat. B,* 2008, **134**, 166-170.

42. S. Mao, S. Cui, G. Lu, K. Yu, Z. Wen and J. Chen, *J. Mater. Chem.*, 2012, **22**, 11009-11013.

43. P. Sun, X. Zhou, C. Wang, B.Wang, X. Xu and G. Lu, *Sens. Actuat. B*, 2014, **190**, 32-39.

44. M. Takata, D. Tsubone and H. and Yanagida, *J. Am. Ceram. Soc.,* 1976, **59**, 4-8.

45. T. Tsuboi, K. Ishii and S. Tamura, Proceedings of the 17th International Colloquium on the Dynamics of Explosions and Reactive Systems, 1999.

46. Y. Nakamura, H. Yoshioka, M. Miyayama and H. Yanagida, *J. Electrochem. Soc.,* 1990, **137**, 940-943.

47. Y. Chang, Y. Yao, B. Wang, H. Luo, T. Li, L. Zhi, *J. Mater. Sci. Technol.,* 2013, **29**, 157-160.

48. K. P. Loh, Q. Bao, P. K. Ang and J. Yang, *J. Mater. Chem.,* 2010, **20**, 2277-2289.

49. W. S. Hummers and R.E. Offeman, *J. Am. Chem. Soc.*, 1958, **80**, 1339.

50. N. I. Kovtyukhova, P. J. Ollivier, B. R. Martin, T. E. Mallouk, S. A. Chizhik, E. V. Buzaneva and A. D. Gorchinskiy, *Chem. Mater.*, 1999, **11**, 771-778.

51. J. Li, J. Zhu and X. Liu, *New J. Chem.*, 2013, **37**, 4241-4249.

52. S. Liang, J. Zhu, C. Wang, S. Yu, H. Bi, X. Liu and X. Wang, *Appl. Surf. Sci.*, 2014, **292**, 278-284.

Graphical Abstract

Reduced Graphene Oxide Decorated with CuO-ZnO Hetero-Junctions: towards High Selective Gas-Sensing Property to Acetone

Chao Wang, Junwu Zhu*, Shiming Liang, Huiping Bi, Qiaofeng Han, Xiaoheng Liu, Xin Wang*

The CuO-ZnO/rGO ternary composite is successfully prepared, in which valid p-n junctions exist between CuO and ZnO nanoparticles with the aid of rGO sheets. The presence of p-n junctions enables such composite to possess outstanding sensing properties to acetone and superior performance for effectively distinguishing acetone and ethanol, that are key features for gas sensor device.